

Finite Element Solution of the Two-Dimensional Bates Model for Option Pricing Under Stochastic Volatility and Jumps

Neda Bagheri Renani¹ and Daniel Ševčovič²

Department of Applied Mathematics and Statistics, Comenius University in Bratislava, Slovakia^{1,2};
neda.bagheri@fmph.uniba.sk¹, sevcovic@fmph.uniba.sk²

Abstract. We propose a fourth-order compact finite-difference (HOC-FD) scheme for the transformed Bates partial integro-differential equation (PIDE). The method employs an implicit-explicit (IMEX) Crank-Nicolson framework for local terms and Simpson quadrature for the jump integral. Benchmarks against second-order finite differences (FD) and quadratic finite elements (FEM, $p = 2$) confirm near-fourth-order spatial accuracy for HOC-FD, near-second-order for FEM, and second-order temporal convergence for all time integrators. Efficiency tests show that HOC-FD achieves similar accuracy at up to two orders of magnitude lower runtime than FEM, establishing it as a practical baseline for option pricing under stochastic volatility jump-diffusion models.

Keywords: Bates model; option pricing; partial integro-differential equation (PIDE); high order compact finite difference; finite element method

1 Introduction

Stochastic volatility models with jumps, such as the Bates model, lead to partial integro-differential equations (PIDEs) central to option pricing. Their complexity motivates efficient high-order numerical solvers [8, 9]. Compact high-order finite difference schemes have been successfully applied to liquidity shock models [15], nonlinear PDEs [13], fractional extensions [10], and uncertain correlation problems [14], confirming their advantages for accuracy and stability.

We develop a fourth-order compact finite-difference (HOC-FD) scheme for the transformed Bates PIDE, combining an IMEX-Crank-Nicolson split for local terms with Simpson quadrature for the jump integral. Benchmarks against second-order finite differences and quadratic FEM demonstrate near fourth-order spatial accuracy, second-order temporal accuracy, and substantial efficiency gains, establishing HOC-FD as a competitive baseline for option pricing under stochastic volatility jump-diffusion models.

2 Stochastic Differential Equations of the Bates Model

The Bates model augments the Heston stochastic–volatility framework with a jump component in the asset price, combining continuous variance dynamics with discontinuous returns to better reproduce market skew, fat tails, and smile effects ([2, 6, 23] see also [9]).

Risk–neutral dynamics. Let $S(t)$ denote the price of the asset and $v(t)$ the variance. Under the risk–neutral measure with correlation ρ between Brownian drivers,

$$\begin{aligned} dS(t) &= \mu S(t)dt + \sqrt{v(t)}S(t)dW_S(t) + S(t)dJ(t), \\ dv(t) &= \kappa(\theta - v(t))dt + \sigma\sqrt{v(t)}dW_v(t), \end{aligned}$$

where $\kappa > 0$ (mean–reversion speed), $\theta > 0$ (long–run variance), and $\sigma > 0$ (volatility of variance). The jump process $J(t)$ is Poisson with intensity λ ; logarithmic jump sizes Y are often modeled Gaussian with mean μ_J and variance σ_J^2 , yielding multiplicative price jumps $S \mapsto Se^Y$ [11, 19].

Option–pricing PIDE. For an option value $V(S, v, t)$ with a risk–free rate r , the price satisfies the partial integro–differential equation:

$$\begin{aligned} \frac{\partial V}{\partial t} + \frac{1}{2}S^2v\frac{\partial^2 V}{\partial S^2} + \rho\sigma vS\frac{\partial^2 V}{\partial S\partial v} + \frac{1}{2}\sigma^2v\frac{\partial^2 V}{\partial v^2} + (r - \lambda)S\frac{\partial V}{\partial S} + \kappa(\theta - v)\frac{\partial V}{\partial v} \\ - (r + \lambda)V = \lambda \int_{\mathbb{R}} \left[V(Se^z, v, t) - V(S, v, t) - (e^z - 1)S\frac{\partial V}{\partial S}(S, v, t) \right] f(z) dz. \end{aligned}$$

where $f(z)$ is the density of the log–jump size z (e.g., Gaussian with mean μ_J and variance σ_J^2), where $f(z)$ denotes the density of the log jump size z (typically $z \sim \mathcal{N}(\mu_J, \sigma_J^2)$) [4, 5].

2.1 Transformed Bates Model PIDE

To obtain a numerically convenient form, we introduce the backward time and normalized variables.

$$\tau = T - t \quad x = \ln \frac{S}{K} \quad y = \frac{\sigma}{v} \quad u(x, y, \tau) = \frac{1}{K} e^{(r+\lambda)\tau} V(S, v, t).$$

Here, K is the strike, r the risk–free rate, and the parameter $\lambda > 0$ measures the intensity of jumps. Let $f(z)$ denote the probability density of the logarithmic jump size [11, 20]. With these variables and using differentiation rules, we have:

$$\begin{aligned} S\frac{\partial}{\partial S} &= \frac{\partial}{\partial x}, \quad v\frac{\partial}{\partial v} = -y\frac{\partial}{\partial y}, \quad S^2\frac{\partial^2}{\partial S^2} = \frac{\partial^2}{\partial x^2} - \frac{\partial}{\partial x}, \quad v\frac{\partial}{\partial v} = -y\frac{\partial}{\partial y}, \\ v\frac{\partial^2}{\partial v^2} &= \frac{y^3}{\sigma}\frac{\partial^2}{\partial y^2} + 2\frac{y^2}{\sigma}\frac{\partial}{\partial y}, \quad vS\frac{\partial^2}{\partial S\partial v} = -y\frac{\partial^2}{\partial x\partial y}, \end{aligned}$$

$$\frac{\partial V}{\partial t} - (r + \lambda)V = -K e^{-(r+\lambda)\tau} \frac{\partial u}{\partial \tau}, \quad V(Se^z, v, t) = K e^{-(r+\lambda)\tau} u(x + z, y, \tau).$$

Thus, the transformed PIDE reads as follows:

$$\begin{aligned} & -\frac{\partial u}{\partial \tau} + \frac{\sigma}{2y} \left(\frac{\partial^2 u}{\partial x^2} - \frac{\partial u}{\partial x} \right) - \rho\sigma y \frac{\partial^2 u}{\partial x \partial y} + \frac{\sigma}{2} \left(y^3 \frac{\partial^2 u}{\partial y^2} + 2y^2 \frac{\partial u}{\partial y} \right) \\ & + (r - \lambda) \frac{\partial u}{\partial x} - \kappa \left(\theta - \frac{\sigma}{y} \right) \frac{y^2}{\sigma} \frac{\partial u}{\partial y} \\ & + \lambda \int_{\mathbb{R}} \left[u(x + z, y, \tau) - u(x, y, \tau) - (e^z - 1) \frac{\partial u}{\partial x}(x, y, \tau) \right] f(z) dz = 0. \end{aligned} \quad (1)$$

3 Spatial Discretization and IMEX–Crank–Nicolson

We consider a uniform tensor product grid $\{(x_i, y_j) : i = 0, \dots, N_x, j = 0, \dots, N_y\}$, $x_i = x_{\min} + i h_x$, $y_j = y_{\min} + j h_y$, with spatial discretization steps $h_x, h_y > 0$. Let $u_{i,j}^n$ denote the approximation to $u(x_i, y_j, \tau_n)$ at time levels $\tau_n = nk$, where $k = T/N_\tau$. The center difference operators $D_x, D_y, D_{xx}, D_{yy}, D_{xy}$ will be used for the spatial derivatives (their concrete stencils are given in Sections 3.1–3.2). The local (differential) part of (1) reads as:

$$L[u] = \frac{\sigma}{2y} u_{xx} + \frac{\sigma}{2} y^3 u_{yy} - \rho\sigma y u_{xy} + \left(r - \lambda - \frac{\sigma}{2y} \right) u_x + \left(\sigma y^2 + \kappa y - \kappa \theta \frac{y^2}{\sigma} \right) u_y.$$

Its discrete counterpart at (x_i, y_j) is

$$\begin{aligned} L_h[u]_{i,j} &= \frac{\sigma}{2y_j} D_{xx}u + \frac{\sigma}{2} y_j^3 D_{yy}u - \rho\sigma y_j D_{xy}u + \left(r - \lambda - \frac{\sigma}{2y_j} \right) D_xu \\ &+ \left(\sigma y_j^2 + \kappa y_j - \kappa \theta \frac{y_j^2}{\sigma} \right) D_yu. \end{aligned}$$

The nonlocal (jump) term in (1) is treated explicitly. Its discrete approximation $I_h[u]_{i,j}$ is designed to match the integral part in (1):

$$I_h[u]_{i,j} = \lambda \int_{\mathbb{R}} \left(u(x_i + z, y_j, \tau) - u(x_i, y_j, \tau) - (e^z - 1) u_x(x_i, y_j, \tau) \right) f(z) dz.$$

With these definitions, the semi-discrete system has the form

$$\frac{du}{d\tau} u = L_h[u] + I_h[u].$$

For time stepping, we use an IMEX–Crank–Nicolson scheme: the local operator L_h is treated implicitly, and the jump operator I_h explicitly. Writing U^n for the vector of all grid values at time τ_n , one step from n to $n + 1$ is given by

$$\frac{U^{n+1} - U^n}{k} = \frac{1}{2} L_h[U^{n+1} + U^n] + I_h[U^n].$$

Sections 3.1 and 3.2 provide the compact spatial stencils for L_h and the quadrature/convolution realization of I_h , respectively (cf. [4, 11, 23]).

3.1 Fourth-Order Compact Discretization of the Local Operator

We denote $u_{i,j} \approx u(x_i, y_j, \tau)$ and adopt fourth-order compact relations to approximate first-, second-, and mixed derivatives on a 3×3 stencil. Such compact schemes are well established for elliptic and parabolic PDEs with variable coefficients and are known for their spectral-like resolution [11, 17, 21, 22].

Compact line relations (1D, fourth order). For fixed j (differentiation in x),

$$\frac{1}{4}u_{x,i-1,j} + u_{x,i,j} + \frac{1}{4}u_{x,i+1,j} = \frac{u_{i+1,j} - u_{i-1,j}}{2h_x}, \quad (2)$$

$$\frac{1}{12}u_{xx,i-1,j} + \frac{10}{12}u_{xx,i,j} + \frac{1}{12}u_{xx,i+1,j} = \frac{u_{i-1,j} - 2u_{i,j} + u_{i+1,j}}{h_x^2}. \quad (3)$$

For fixed i (differentiation in y),

$$\frac{1}{4}u_{y,i,j-1} + u_{y,i,j} + \frac{1}{4}u_{y,i,j+1} = \frac{u_{i,j+1} - u_{i,j-1}}{2h_y}, \quad (4)$$

$$\frac{1}{12}u_{yy,i,j-1} + \frac{10}{12}u_{yy,i,j} + \frac{1}{12}u_{yy,i,j+1} = \frac{u_{i,j-1} - 2u_{i,j} + u_{i,j+1}}{h_y^2}. \quad (5)$$

Mixed derivative via sequential compact differentiation. Let $M_x = \text{tridiag}(\frac{1}{4}, 1, \frac{1}{4})$ and D_x the centered difference line operator in x , with M_y, D_y defined analogously. The mixed derivative is evaluated by

$$U_{xy} = M_x^{-1}D_x(M_y^{-1}D_yU) = M_y^{-1}D_y(M_x^{-1}D_xU).$$

Compact local operator (nodewise form). With coefficients taken directly from the transformed Bates operator (1), we have

$$(L_h[U])_{i,j} = a_{i,j}U_{xx} + b_{i,j}U_{yy} + c_{i,j}U_{xy} + d_{i,j}U_x + e_{i,j}U_y + f_{i,j}U_{i,j}, \quad (6)$$

where

$$\begin{aligned} a_{i,j} &= \frac{1}{2} \frac{\sigma}{y_j}, & b_{i,j} &= \frac{1}{2} \sigma y_j^3, & c_{i,j} &= -\rho \sigma y_j, & d_{i,j} &= (r - \lambda) - \frac{1}{2} \frac{\sigma}{y_j}, \\ e_{i,j} &= \sigma y_j^2 + \kappa y_j - \kappa \theta \frac{y_j^2}{\sigma}, & f_{i,j} &= 0. \end{aligned}$$

Here $U_x, U_y, U_{xx}, U_{yy}, U_{xy}$ are supplied by the compact relations (2)–(5) and the mixed construction above. The interior accuracy satisfies

$$L_h[u] - L[u] = O(h_x^4 + h_y^4).$$

Nine-point compact balance (assembled stencil). Eliminating auxiliary derivatives from (2)–(5) within (6) yields a 3×3 balance

$$\sum_{\ell=0}^8 \alpha_{\ell} u_{\ell} = \sum_{\ell=0}^8 \gamma_{\ell} f_{\ell},$$

with $\{u_{\ell}\}$ the stencil values centered at (i, j) and $\{f_{\ell}\}$ the right-hand side samples (arising from PDE insertion at (i, j)). The weights $\alpha_{\ell}, \gamma_{\ell}$ depend only on the local coefficients and (h_x, h_y) .

Verification template (constant coefficients). For $a = b = 1, c = d = e = 0, h_x = h_y = h$, the scheme reduces to the classical fourth-order nine-point Laplacian [1, 7]

$$\begin{aligned} & \frac{-u_{i-1,j-1} + 16u_{i,j-1} - u_{i+1,j-1} + 16u_{i-1,j} - 60u_{i,j} + 16u_{i+1,j}}{12h^2} \\ & + \frac{-u_{i-1,j+1} + 16u_{i,j+1} - u_{i+1,j+1}}{12h^2} = f_{i,j} + \frac{h^2}{12} \Delta f_{i,j}. \end{aligned}$$

providing a convenient code check in line with established compact formulations for financial PIDEs [2, 3, 11, 12, 18].

3.2 Nonlocal Jump Operator and IMEX–CN Time Marching

The nonlocal jump part of (1) is

$$\lambda \int_{\mathbb{R}} [u(x+z, y, \tau) - u(x, y, \tau) - (e^z - 1)u_x(x, y, \tau)] f(z) dz,$$

with log-normal jump density $f(z)$ [5, 7, 19]. The compensator $(e^z - 1)u_x$ guarantees integrability and preserves the martingale condition.

Discrete jump operator. On the grid, we approximate

$$(I_h[u])_{i,j} = \lambda \sum_{m=-M}^M \omega_m [u(x_i + z_m, y_j, \tau) - u(x_i, y_j, \tau) - (e^{z_m} - 1)D_x u(x_i, y_j, \tau)],$$

using quadrature nodes $\{z_m\}$ and weights $\{\omega_m\}$, with interpolation for off-grid values [7, 11, 18].

IMEX–CN scheme. The semi-discrete system

$$\frac{d}{d\tau} U = L_h[U] + I_h[U]$$

is advanced in time by the IMEX–Crank–Nicolson method [2, 16]:

$$\frac{U^{n+1} - U^n}{k} = \frac{1}{2} L_h[U^{n+1} + U^n] + I_h[U^n],$$

treating L_h implicitly and I_h explicitly. This combination retains unconditional stability for the stiff diffusion operator while avoiding costly implicit treatment of the integral. The scheme fits naturally into high-order compact PIDE solvers [11, 12, 21].

4 Initial and Boundary Conditions

For the transformed Bates PIDE we prescribe the payoff as the initial condition at $\tau = 0$:

$$u(x, y, 0) = \max(1 - e^x, 0).$$

At the far left boundary x_{\min} , the option value approaches the discounted intrinsic value. Thus we impose

$$u(x_{\min}, y, \tau) = e^{(r+\lambda)\tau} (1 - e^{x_{\min}}).$$

At the far right boundary x_{\max} , the put option value decays, so we set:

$$u(x_{\max}, y, \tau) = 0.$$

In the variance direction, we impose homogeneous Neumann conditions:

$$\partial_y u(x, y_{\min}, \tau) = 0, \quad \partial_y u(x, y_{\max}, \tau) = 0.$$

These conditions ensure consistency with the no-arbitrage bounds for European puts under stochastic volatility jump–diffusion dynamics.

5 Benchmarking via the Finite Element Method

We benchmark the compact finite-difference scheme against a conforming finite element method (FEM) applied to the transformed Bates PIDE under identical payoff and boundary conditions. The comparison highlights accuracy, stability, and computational cost.

Weak formulation. Writing the local operator in divergence form, we enforce economic Dirichlet conditions on vertical boundaries and homogeneous Neumann conditions on horizontal ones, consistent with the FD setup. The weak form reads

$$\left(\frac{u^{n+1} - u^n}{\Delta\tau}, \psi \right) + a \left(\frac{u^{n+1} + u^n}{2}, \psi \right) = \left(\frac{3}{2} L_I[u^n] - \frac{1}{2} L_I[u^{n-1}], \psi \right), \quad \forall \psi \in V,$$

with $V = \{\psi \in H^1(\Omega) : \psi|_{\Gamma_D} = 0\}$ and bilinear form

$$a(u, \psi) = \int_{\Omega} A \nabla u \cdot \nabla \psi \, dx dy + \int_{\Omega} (b \cdot \nabla u) \psi \, dx dy.$$

Spatial discretization. In a regular shape mesh we use $V_h \subset V$ with continuous quadratic elements (P2/Q2). The Gaussian quadrature yields the mass M , stiffness K , and convection C matrices. For coefficient vector U^n ,

$$A_h U^{n+1} = B_h U^n + \Delta\tau \left(\frac{3}{2} F^n - \frac{1}{2} F^{n-1} \right),$$

with $A_h = M + \frac{\Delta\tau}{2}(K + C)$, $B_h = M - \frac{\Delta\tau}{2}(K + C)$, and $F^n = (L_I[u_h^n], \phi_i)$. For time-independent coefficients, a sparse factorization of A_h is reused.

Jump treatment. The nonlocal operator is evaluated explicitly by Simpson quadrature on a truncated log-jump interval, with FEM interpolation at off-grid x -values. This keeps the implicit system confined to local terms.

Takeaway. FEM achieves near second-order spatial convergence for quadratic elements [4, 23, 24], but in structured domains HOC–FD attains comparable accuracy with significantly lower runtime and memory [11, 21].

6 Numerical Experiments

We evaluate the (HOC–FD) scheme for the transformed Bates PIDE against second–order finite differences and FEM with Lagrange bases of degree $p = 1, 2$. All solvers employ identical payoff and boundary conditions, the IMEX–CN scheme for local terms, and explicit Simpson quadrature on a truncated interval for the jump integral. Accuracy is measured by discrete L^2 error and RMSE relative to a high–resolution reference, while efficiency is assessed in terms of degrees of freedom, CPU time, memory usage, and a cost–accuracy ratio.

Table 1. Simulation parameters used in Bates model experiments

Parameter	Value	Parameter	Value	Parameter	Value
K	110	T (years)	1.0	r	0.03
κ	1.8	θ	0.02	ρ	−0.4
σ	0.15	λ	0.25	Jump law	Lognormal
μ_J	set per exp.	σ_J	set per exp.	–	–

6.1 Numerical Convergence

We measure numerical accuracy using three error norms:

$$\|u^h - u^{ref}\|_{L^2} = \left(h_x h_y \sum_{i=1}^{N_x} \sum_{j=1}^{N_y} (u_{i,j}^h - u_{i,j}^{ref})^2 \right)^{1/2},$$

the discrete L^2 error norm, which approximates the continuous integral norm;

$$\text{RMSE} = \left(\frac{1}{N_x N_y} \sum_{i=1}^{N_x} \sum_{j=1}^{N_y} (u_{i,j}^h - u_{i,j}^{ref})^2 \right)^{1/2},$$

the root-mean-square error, representing average nodal error; and

$$\|u^h - u^{ref}\|_{L^\infty} = \max_{1 \leq i \leq N_x, 1 \leq j \leq N_y} |u_{i,j}^h - u_{i,j}^{ref}|,$$

the maximum pointwise error.

Thus, L^2 reflects global accuracy, RMSE captures average nodal error, and L^∞ highlights the worst-case deviation [2, 16, 23].

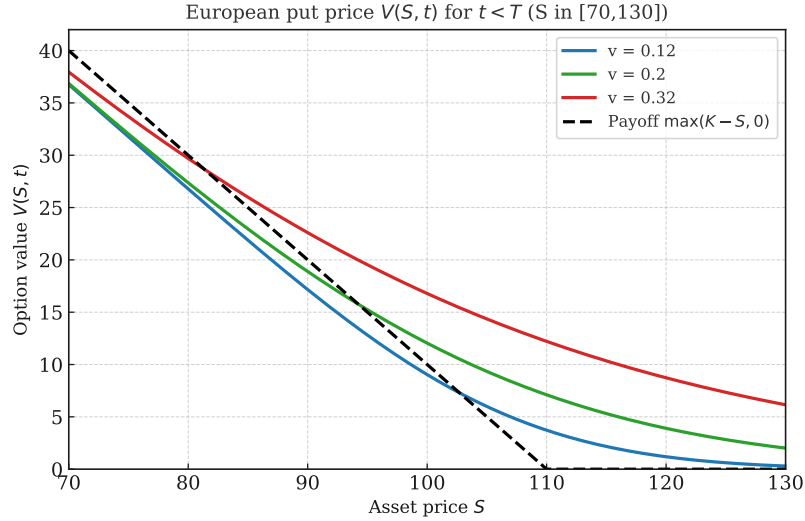


Fig. 1. European put price $V(S, t)$ under the Bates model for $S \in [70, 130]$. The intrinsic payoff $\max(K - S, 0)$ and the no-arbitrage lower bound $\max\{Ke^{-rT} - S, 0\}$ are shown as reference curves

Table 2. Observed convergence orders in space and time, comparing HOC–FD with second–order finite differences [2, 7] and FEM(P2) [4, 23, 24]. Spatial studies fix $\Delta\tau/h^2$; temporal studies fix h

Method	Spatial order p_s	Temporal order p_t
FEM (P2)	≈ 2.0 (both L^2, L^∞)	≈ 2.0 (CN, BDF2, MP)
HOC–FD (compact)	≈ 4.0 (both L^2, L^∞)	≈ 2.0 (IMEX–CN)

6.2 Computational Efficiency Comparison

Efficiency was assessed using the cost–accuracy ratio

$$\eta_{A/B} = \frac{\varepsilon_A^2 t_A}{\varepsilon_B^2 t_B}, \quad \varepsilon \in \{\|\cdot\|_{L^2}, \text{RMSE}\},$$

reported relative to the HOC–FD baseline ($\eta = 1$). Here t denotes CPU time.

Table 3 shows that, at matched settings, the compact HOC–FD scheme attains comparable accuracy at substantially lower runtime on structured grids. Relative to HOC–FD, FEM(P2) is roughly two orders of magnitude more costly, while second–order FD variants are within single–digit multiples of the baseline. These results confirm earlier findings that compact FD schemes achieve significant efficiency gains over FEM in structured domains [4, 11, 24].

Table 3. Efficiency snapshot at $h = 0.1$ relative to HOC-FD baseline [11, 21]. Comparisons include second-order finite differences [2, 7] and FEM(P2) [4, 23, 24]. Errors measured against a high-resolution reference; η uses L^2 error and runtime

Method	DOF	Time (s)	L^2	RMSE	η
HOC-FD (IMEX-CN)	1,681	1.106	0.0230	0.0095	1.00
FEM (P_2)	6,561	23.426	0.1522	0.0475	$\approx 1.40 \times 10^2$
CN (2nd-order FD)	1,681	2.230	0.0341	0.0148	≈ 2.99
BDF2 (2nd-order FD)	1,681	2.904	0.0417	0.0181	≈ 4.76
Midpoint (FD)	1,681	3.117	0.0425	0.0185	≈ 5.21

7 Conclusion

We developed a fourth-order compact finite-difference scheme for the transformed Bates PIDE, combining an IMEX-Crank-Nicolson split for local terms with explicit Simpson quadrature for the jump integral. Benchmarks against second-order finite differences and quadratic FEM confirmed near-fourth-order spatial accuracy for the compact scheme and near-second-order for FEM, with all time integrators exhibiting second-order accuracy. Efficiency tests on structured grids showed that the compact scheme achieves substantially lower runtimes—up to two orders of magnitude faster than FEM—while maintaining comparable pricing accuracy. This establishes the scheme as a competitive baseline for structured-domain option pricing. Future work will extend the method to American and path-dependent payoffs, adaptive meshes, broader jump specifications, and accelerated integral solvers.

8 Acknowledgements

The first author was supported by Comenius University grant UK/1024/2025. The second author received support from the Slovak VEGA 1-0493-24 agency.

References

1. Achdou, Y., Franchi, B., Tehou, N.: A partial differential equation connected to option pricing with stochastic volatility: regularity results and discretization. *Mathematics of Computation* 74(251), 1291–1322 (2005)
2. Bagheri, N., Haghghi, H.K.: A comparison study of adi and lod methods on option pricing models. *Journal of Mathematical Finance* 7(2), 275–290 (2017)
3. Balajewicz, M., Toivanen, J.: Reduced order models for pricing european and american options under stochastic volatility and jump-diffusion models. *Journal of Computational Science* 20, 198–204 (2017)
4. Ballestra, L.V., Sgarra, C.: The evaluation of american options in a stochastic volatility model with jumps: An efficient finite element approach. *Computers & Mathematics with Applications* 60(6), 1571–1590 (2010)
5. Bates, D.S.: Jumps and stochastic volatility: Exchange rate processes implicit in deutsche mark options. *The Review of Financial Studies* 9(1), 69–107 (1996)

6. Black, F., Scholes, M.: The pricing of options and corporate liabilities. *Journal of Political Economy* 81(3), 637–654 (1973)
7. Cont, R., Voltchkova, E.: A finite difference scheme for option pricing in jump diffusion and exponential lévy models. *SIAM Journal on Numerical Analysis* 43(4), 1596–1626 (2005)
8. Cruz, J.M.T.S., Ševčovič, D.: On solutions of a partial integro-differential equation in bessel potential spaces with applications in option pricing models. *Japan Journal of Industrial and Applied Mathematics* 37(3), 697–721 (2020)
9. Cruz, J.M., Ševčovič, D.: Option pricing in illiquid markets with jumps. *Applied Mathematical Finance* 25(4), 395–415 (2018)
10. Dimitrov, D., Vulkov, L.: High order finite difference schemes on non-uniform meshes for the time-fractional black–scholes equation. *Applied Numerical Mathematics* 111, 251–266 (2016)
11. Düring, B., Pitkin, A.: High-order compact finite difference scheme for option pricing in stochastic volatility jump models. *Journal of Computational and Applied Mathematics* 355, 201–217 (2019)
12. Düring, B., Pitkin, A.: Efficient hedging in bates model using high-order compact finite differences. arXiv preprint arXiv:1710.05542 (2024)
13. Koleva, M.N., Vulkov, L.G.: A kernel-based algorithm for numerical solution of nonlinear pdes in finance. In: *Numerical Analysis and Its Applications (NAA 2012)*, Lecture Notes in Computer Science, vol. 8236, pp. 520–527. Springer (2013)
14. Koleva, M.N., Vulkov, L.G.: A positive flux limited difference scheme for option pricing 2d fully non-linear parabolic equation with uncertain correlation. *Journal of Computational and Applied Mathematics* 271, 368–382 (2014)
15. Koleva, M.N., Vulkov, L.G., Mudzimbabwe, T.: Fourth-order compact schemes for a parabolic-ordinary system of european option pricing liquidity shocks model. *Numerical Algorithms* 74, 1075–1098 (2017)
16. Kreiss, H.O.: Initial boundary value problems for hyperbolic systems. *Communications on Pure and Applied Mathematics* 23(3), 277–298 (1970)
17. Lele, S.K.: Compact finite difference schemes with spectral-like resolution. *Journal of Computational Physics* 103(1), 16–42 (1992)
18. Mao, M., Tian, H., Wang, W.: A variable step-size extrapolated crank–nicolson method for option pricing under stochastic volatility model with jump. *Mathematical Methods in the Applied Sciences* 47(2), 762–781 (2024)
19. Merton, R.C.: Option pricing when underlying stock returns are discontinuous. *Journal of Financial Economics* 3(1-2), 125–144 (1976)
20. Pankratov, E.: Nonlinear profit maximization with account changing of prices. *International journal of modeling, simulation and applications* 2(2), 9–17 (2018)
21. Pitkin, A.: High-order compact finite difference schemes for option pricing in stochastic volatility jump-diffusion models. Ph.D. thesis, University of Sussex (2020)
22. Spotz, W.F., Carey, G.F.: A high-order compact formulation for the 3d poisson equation. *Numerical Methods for Partial Differential Equations: An International Journal* 12(2), 235–243 (1996)
23. Thomée, V.: *Galerkin finite element methods for parabolic problems*, vol. 25. Springer Science & Business Media (2007)
24. Uzunca, M., et al.: Pricing european and american options under heston model using discontinuous galerkin finite elements. Tech. rep., arXiv.org (2020)